ROYAL SOCIETY OF CHEMISTRY

REVIEW

Check for updates

Chemistry and properties of fluorescent pyrazole derivatives: an approach to bioimaging applications†

Santiago Melo-Hernández, María-Camila Ríos and Jaime Portilla [ID] *

Fluorescent bioimaging is a crucial technique for *in vivo* studies in real cell samples, providing vital information about the metabolism of ions or molecules of biological and pharmaceutical significance. This technique typically uses probes based on organic small-molecule fluorophores, with N-heteroaromatic scaffolds playing an essential role due to their exceptional electronic properties and biocompatibility. Among these, pyrazole derivatives stand out as particularly promising due to their high synthetic versatility and structural diversity. This review highlights prominent examples from the period 2020–2024, focusing on the chemistry, properties, and bioimaging applications of fluorescent pyrazole derivatives. By highlighting the latest advancements in this field, this manuscript aims to inspire and motivate researchers, emphasizing the potential impact of this work on the future of bioimaging.

1   Introduction

In recent years, non-invasive optical techniques, such as fluorescence-based bioimaging, have emerged as rapid and efficient tools for real-time monitoring of biological processes in live tissues and cells.[1–3] These methods are crucial for both basic biological research and clinical applications, including therapeutic and diagnostic purposes, as they enable the testing

Bioorganic Compounds Research Group, Department of Chemistry, Universidad de Los Andes, Carrera 1 No. 18A-10, Bogotá 111711, Colombia. E-mail: jportill@uniandes. edu.co

† Electronic supplementary information (ESI) available. See DOI: https://doi.org/10.1039/d4ra07485h

of metabolic processes and the monitoring of the changes in biochemical indicators and biomarkers. The obtained results can be achieved using affordable and user-friendly devices such as fluorescence and confocal microscopes.[4–6] Applications of these methods include general cell staining,[7–9] labelling of subcellular structures,[10–12] and the detection of ions or small molecules, such as Cu^{2+}, reactive oxygen species, and reactive nitrogen species (ROS or RNS).[13–17] These techniques also facilitate the assessment of intracellular conditions, including pH[18–20] and hypoxia,[21–23] which are important for sensing cancer,[24–26] bacterial infections,[27–29] ischemic injury,[30–32] and even for theragnostics (a combination of therapy and diagnostics).[33–35] When a bioimage is required for detection, the

Santiago Melo-Hernandez was born in Bogotá (Colombia) and received BSc degrees in Chemistry (2020) and Microbiology (2021), both at the Universidad de Los Andes (Bogotá). Currently, he works as a patent advisor at a law firm, being in close contact with the latest developments in different industries, especially in the pharmaceutical and biotechnology fields. His research interest focuses on synthesising

Santiago Melo-Hernández

compounds with potential biological activity and biological evaluation to develop new therapeutic and/or diagnostic leads.
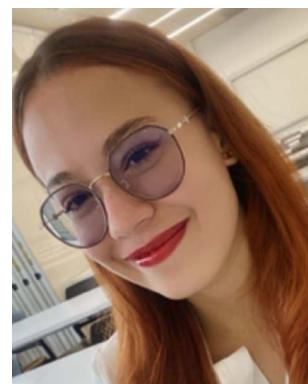
Maria-Camila Rios was born in Medellin (Colombia); she received her BSc degree in 2021 and her MSc in 2024 at the Universidad de Los Andes (Bogotá). Currently, she works as a research assistant at the bioorganic compounds research group in the same institution under the supervision of Prof. Jaime Portilla. Her research interest focuses on synthesising heterocyclic compounds with biological or photophysical

María-Camila Ríos

relevance.

sensing can be achieved by monitoring changes in fluorescence, either a turn-on or turn-off response, resulting from the interaction of the probe with the target analyte or cells[1,2,4,5] (Fig. 1a).

Considering the broad scope of applicability described above, there has been significant interest from both academia and industry in developing suitable systems, platforms, and methodologies for bioimaging applications.[1–35] However, it remains challenging to identify novel, highly sensitive, and selective probes with good physiological compatibility.[36–38] Many fluorescent scaffolds have been explored to develop new molecular probes tailored for bioimaging in this field. Various reported fluorophores include those containing heterocyclic rings, such as coumarin,[39,40] boron complexes (*e.g.*, BODIPY),[41,42] and N-heteroaromatic cores (*e.g.*, pyrroles, diazoles, pyridines, diazines, *etc.*).[17,43,44] Additionally, probes based on aromatic hydrocarbons (*e.g.*, indane, naphthalene, pyrene, tetraphenylethene, among others) have also been explored, despite their relatively lower biocompatibility[34,45–47] (Fig. 1b).

Fluorophores based on N-heteroaromatic cores have been extensively explored for various biological and photophysical applications, as the heteroatom imparts important electronic properties to the probes. These compounds are usually stable[17,43,44] and exhibit excellent synthetic versatility, particularly in terms of ring construction and subsequent functionalization reactions.[43,44,48,49] Thus, exploration of fluorescent N-heterocyclic compounds remains an ongoing challenge, with continuous efforts aimed at improving their scope and applicability. Many organic compounds have been widely studied in the field of organic materials in recent years,[43,50,51] leading to the successful application of porphyrins,[52,53] polypyrroles,[54] boron dipyrrolomethane (BODIPY),[55,56] and certain 5 : 6 aza-fused diazoles with key dipolar motifs[57–59] (Fig. 2a). Specifically, diverse pyrazole derivatives have shown fluorescent properties with high quantum yields and good photostability, thermostability, solvatofluorochromism, *etc.*;[38,60–62] however, what stands out most in pyrazole derivatives is their high synthetic versatility, from the construction of the simple and fused ring to the functionalization reactions of the same[43,63–65] (Fig. 2b).

Considering bioimaging applications, pyrazole derivatives have been reported to have good membrane permeability and biocompatibility, making them suitable as bioactive and biosensing compounds, and, due to their N-donor character,[60–65] also ideal for cation detection *in vivo*.[17,62,66] Many fluorescent pyrazoles for bioimaging purposes have been reported, with the pyrazoline ring being more frequent than the aromatic core; still, their fluorescent property is usually based on their substituents or fused rings (Fig. 2b). Therefore, and as a follow-up to the last review by our group in this regard,[17] this review covers the chronological reports made in the previous five years (2020–2024) on pyrazole derivatives for use in bioimaging. The discussion focuses on analysing five works per year, covering the compounds' syntheses and their bioimaging properties.

To better understand the purpose of this review, Table 1 presents a summary with the most pertinent results for some of the probes analysed. Specifically, five examples matching each of the years explored are shown, in which the syntheses and applications date are detailed. Table 1 and Fig. 2c show how pyrazoline, pyrazole, and fused pyrazole rings are built by cyclization reactions of 1,3-biselectrophilic reagents with hydrazine derivatives; likewise, the appropriate functionalization or derivatization of pyrazoles for different applications is also shown. The primary aim of this work is to share the knowledge gained on the chemistry of pyrazole derivatives and their photophysical pertinency.[17,43,44,62–65] Thus, we hope that
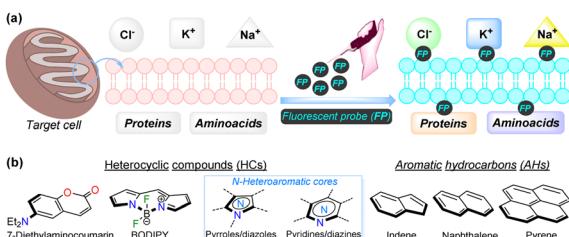

Fig. 1 (a) Pictorial depiction of bioimaging acquisition by fluorescent probes. (b) Structural cores of several fluorophores used for bioimaging.

Jaime Portilla was born in Cali (Colombia); he is a research professor at the Department of Chemistry of the Universidad de Los Andes in Bogotá, where he led the bioorganic compounds research group in 2008. He completed his PhD in Organic Synthesis under the supervision of Prof. J. Quiroga (2007) at the Universidad del Valle (Cali). His current research interests involve the areas of supramolecular chemistry and molecular recognition. His research group focuses on eco-compatible organic synthesis approaches, predominantly in 5 : 6 aza-fused heterocyclic compounds with biological or photophysical potential.

Jaime Portilla
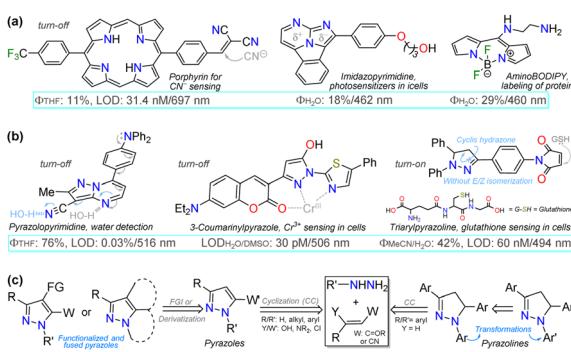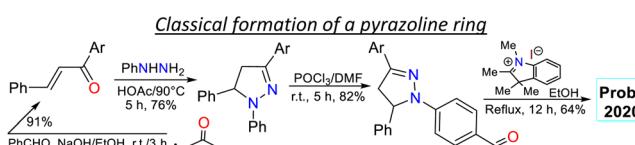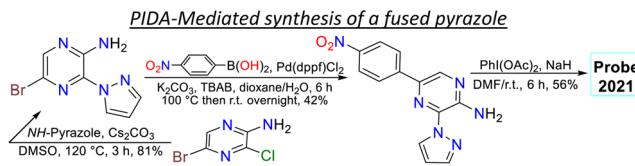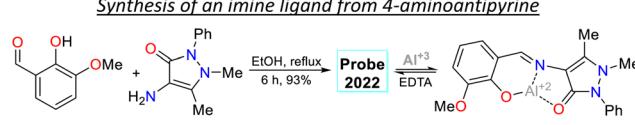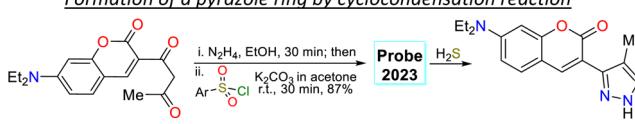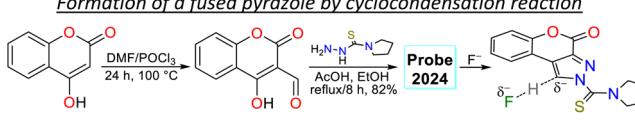
Fig. 2 (a) Structure of some fluorescent N-heterocyclic dyes, (b) applications in detection chemistry, and (c) general syntheses of pyrazole derivatives.

Table 1 Overview of some pyrazole derivatives for bioimaging application of 2020 to 2024[a]

Section, Probe	General probe synthesis	Application data
2.1,	*Classical formation of a pyrazoline ring*	LOD/turn-on = 80 nM at 480 nm in 5% PBS/DMF, Φ = 13% at 640 nm.[67] Mitochondrial sensing
2.2,	*PIDA-Mediated synthesis of a fused pyrazole*	LOD/turn-on = 18.6 ng L^{-1}, Φ = 76%/R-NH$_2$ at 546 nm in DMSO, τ = 6.65 ns.[68] Hypoxia sensing
2.3,	*Synthesis of an imine ligand from 4-aminoantipyrine*	LOD/turn-on = 720 nM at 518 nm in EtOH.[69] Al^{+3} sensing in human colon living cells (HP-29)
2.4,	*Formation of a pyrazole ring by cyclocondensation reaction*	LOD/turn-on = 18.7 nM, Φ = 27% at 500 nm in MeCN.[70] H$_2$S sensing in MCF-7 cells
2.5,	*Formation of a fused pyrazole by cyclocondensation reaction*	LOD = 4.62 nM/turn-on at 492 nm in MeCN.[71] F$^-$ sensing in T24 cells

[a] Complete reaction conditions and yields are shown, which is not always common in article schematics.

this review manuscript will be a helpful contribution to further researchers aiming for novel fluorophores synthesis for bioimaging applications.

2 Articles analysed

2.1. Probes reported in 2020

First, Zhang *et al.*[67] reported the synthesis and long-term bioimaging of the pyrazoline-BODIPY hybrid probe **4** and nanoparticles (NPs) 4-NPs for ultrafast cell staining. Probe **4** was obtained in a 22% yield by the Vilsmeier–Haack reaction of *N*-phenylpyrazoline **1**, yielding the *N*-(4-formylphenyl)pyrazoline **2**. Then, a one-pot reaction of **2** with 2,4-dimethylpyrrole (**3**) and BF$_3$ offered **4**. The probe exhibited an absorption band (λ_{abs}) at 499 nm and an emission band (λ_{em}) at 511 nm with a fluorescence quantum yield (Φ_F) of 30%, attributed to an intramolecular charge transfer (ICT) from the pyrazoline ring to the BODIPY ring. The solvatofluorochromism of **4** showed a blue-shift with a decreased fluorescence intensity in polar solvents; however, an opposite result was observed in non-polar solvents. The rotational restriction around the BODIPY ring indicated a twisted ICT (TICT)-locally excited-state effect, which could explains their findings. This probe showed a high Φ_F in aqueous medium due to an aggregation-induced emission (AIE) process, and it was applied to obtain NPs that were tested on HeLa and

A549 cells, which revealed that the fluorescence intensity had a positive dependency on the time of incubation and concentration of 4-NPs. The *in vivo* fluorescence of the probe injected in the tumours of a mouse model was also explored, staining the tumour for up to 12 days, indicating this was probe suitable for long-term, non-invasive tumour progression monitoring (Scheme 1a).

Subsequently, Wang *et al.*[68] employed probe **7** for *in vivo* sulfite detection in the mitochondria. This probe was
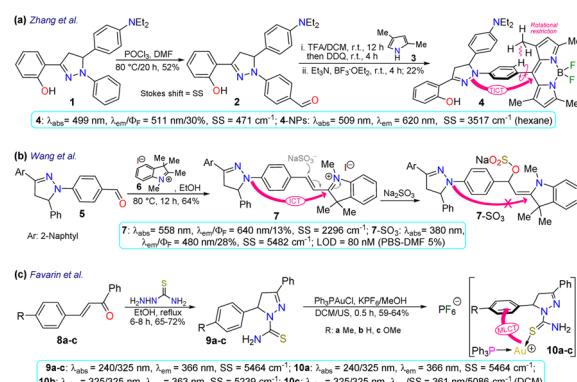
**Scheme 1** Synthesis and optical data of pyrazolines (a) **4**, (b) **7**, and (c) **10a–c**.

synthesised in a 64% yield *via* the condensation of *N*-(4-formylphenyl)pyrazoline with the indolinium salt **6**. The λ_{abs} at 558 nm and λ_{em} at 640 nm with Φ_F of 13% for **6** showed visible changes in the presence of sulfite by interruption of the ICT process due to a break in the π-conjugation upon the anion addition to the salt, acting as a Michael acceptor. The observed changes showed up as a blueshift to 380 nm and 480 nm with a Φ_F of 28%, with a reported limit of detection (LOD) of 80 nM for sulfite. This probe was designed to be located in the mitochondria due to the interaction of the negative charge of the mitochondrial membrane and the positive charge of the indolinium salt, which served as the guiding group. Green emission was observed in the presence of sulfite, indicating that it could efficiently sense exogenous and endogenous sulfite (Scheme 1b).

Favarin *et al.*[69] obtained three gold-based pyrazoline dual probes **10a–c** in 59–64% yields by reacting chloro(triphenylphosphine)gold(I) (Ph₃PAuCl), potassium hexafluorophosphate (KPF₆), and the pyrazoline-based ligands **9a–c**. These ligands exhibited absorption bands around 240 and 325 nm and emission bands around 366 nm, and although they were fluorescent dyes, gold complexes enhanced the emission *via* charge-transfer (CT) processes governed by metal-to-ligand CT (MLCT). The MLCT favoured the intraligand CT (ILCT) and ligand-to-ligand CT (LLCT), as shown by DFT calculations in the ground state, leading the authors to assume that the emission of complexes **10a–c** was due to the mentioned CT processes. However, the photophysical mechanism in the excited state still needs to be studied in more depth as this is less simple. The CT processes led to two λ_{em}, a blue one when excited at about 305 nm and a green one when excited at 405 nm. Cellular imaging was performed on two cancer cell lines (MDA-MD231 and MCF-7) and one non-cancerous healthy cell line (HUVEC). For the studied cell lines, **10a–c** showed good internalisation and staining of the cytoplasm and they seemed to be suitable dyes for general staining or even for co-staining assays, as their dual emission may allow using further dyes that are compatible with at least one of the fluorescence modes of **10a–c**, thereby increasing their span of utility. However, it must be noted that **10a–c** were found to be highly cytotoxic for cancer and non-cancer cell lines, which would impair their application for *in vivo* imaging, as their use would hinder studying cellular processes and lead to the death of the cells (Scheme 1c).

Alizadeh *et al.*[70] used the pyrazolopyridine–coumarin hybrid probes **13a–h** for general cell staining, synthesised in 70–85% yields *via* a 1,3-dipolar cycloaddition reaction of hydrazonoyl chloride **11** and the enone **12**. The reaction proceeded in the presence of ammonium acetate by nucleophilic substitution of the chloride on the coumarin moiety with the nitrogen source, forming an enamine that then reacted with the carbonyl to generate products after aromatization. These probes exhibited coplanar, rigid, and aromatic structures, which were responsible for their fluorescence, except for probes bearing a nitro group as this favoured internal conversion over radiative decay; likewise, the emission spectra were barely affected by the substituents. As a representative example, probe **13a** exhibited
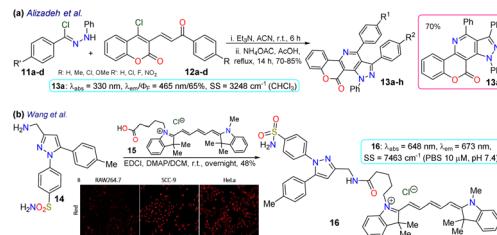

Scheme 2 Synthesis and photophysical data of (a) the fused pyrazoles **13a–h** and (b) the π-extended pyrazole **16**. Bioimage of **16** in RAW264.7, SCC-9, and HeLa cell lines by ref. 71 with minor modifications licensed under Creative Commons CC BY 4.0.

λ_{abs} at 330 nm, λ_{em} at 465 nm, Φ_F of 65%, good photostability, and pH sensitivity; as a result, this probe was applied for the cellular imaging of MG-63 cells. The probe showed good internalisation into the cell, apparently even into the nuclei, as there were no black spots on the images after 30 min of incubation (Scheme 2a).

As a final example in 2020, Wang *et al.*[71] obtained the NIR fluorescent probe celecoxib-based **16** in a 48% yield by the amidation reaction of the 3-aminomethylpyrazole **14** with the carboxylic acid **15** bearing a cyanine moiety. This probe was used in cyclooxygenase sensing 2 (COX-2) in tumoural cells. The photophysical properties of probe **16** were recorded in PBS at pH 7.4 to achieve conditions as close as possible to the cellular environment, displaying λ_{abs} at 648 nm and λ_{em} at 673 nm. In addition, docking studies showed that **16** was a potent inhibitor of COX-2, whose binding site was the same as free celecoxib, *i.e.* inside the active side pocket. The COX-2 inhibiting activity of **16** was confirmed by *in vitro* tests using purified COX-2m, and its actual capability for imaging in living cells was investigated by imaging assays in a normal cell line (RAW264.7) and two cancer cell lines (HeLa and SCC-9). It's very low toxicity to the three cell lines with differential and scarce fluorescence for normal cells but strong fluorescence for cancer cells was evidenced; thus, **16** could discern normal and cancerous cells. As a result, the optical mechanism for **16** must be associated with its accumulation around COX-2, which is less expressed in normal cells, explaining why the RAW264.7 cells barely shined while the cancer cells strongly fluoresced (Scheme 2b).

2.2. Probes reported in 2021

He *et al.*[72] synthesised the (pyrazolin-3-yl) phenyl acrylate **19a–b** in a 50–60% yield by the esterification between 2-(pyrazolin-3-yl)phenol **17a–b** and acryloyl chloride **18**. These probes exhibited very weak emission at 490 nm, but this increased upon the nucleophilic addition of glutathione to the acrylate receptor fragments **19a–b**. Utilising DFT studies, the authors reported that the highest occupied molecular orbital (HOMO) was focused on the *N*-phenylpyrazoline moiety and the lowest unoccupied molecular orbital (LUMO) on the acrylate, causing ICT with fluorescence turn-off; thus, the LUMO was disturbed upon the conjugated addition of the respective thiol group, raising the HOMO–LUMO energy gap and thereby preventing quenching. The probes offered low toxicity, and **19a** was applied
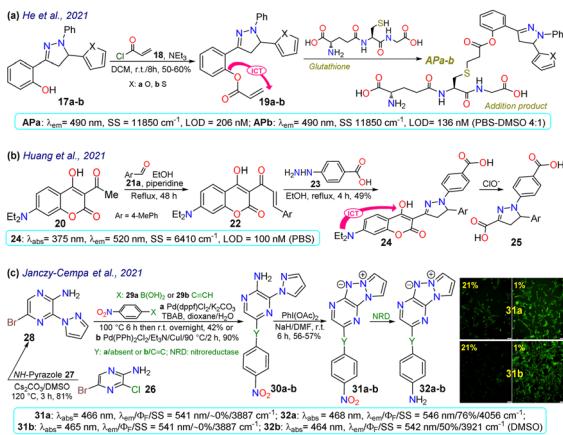
Scheme 3 Synthesis and photophysical data of (a) 19a–b, (b) 24, and (c) 31/32a–b. Bioimaging of A2058 cells cultured under normoxic (21% pO$_2$) and hypoxic (1% pO$_2$) conditions for 24 h with 31a–b (prior 2 h at 8 μM); ref. 73 with minor changes licensed under Creative Commons CC BY 4.0.

for imaging tests in cells cultured with and without glutathione. Incubation of the cells with **19a** led to blue fluorescence inside the cells without any morphological artefacts, indicating that **19a** could detect endogenous glutathione, and has potential as a new tool for studying glutathione's biological role in different processes (Scheme 3a).

Huang et al.[74] obtained the coumarin-3-ylpyrazoline **24** for in vivo hypochlorite sensing by reacting 3-acetylcoumarin **20** with p-tolualdehyde (**21a**) to produce the enone **22**, which then reacted with arylhydrazine **23** to afford **24** in a 49% yield. Probe **24** showed λ_{abs} at 375 nm, λ_{em} at 520 nm, and a donor–acceptor structure from an electron-donating group (EDG), such as diethylamino, to an electron-withdrawing group (EWG), such as hydrazone, in the pyrazoline fragment, favouring the emission of **24** by an ICT phenomenon. This probe was degraded to the dicarboxylic acid **25** through hypochlorite-mediated oxidation upon adding the analyte (on the coumarin ring), quenching its fluorescence. The fluorophore **24** showed slight cytotoxicity and good internalisation into the cytoplasm for cell imaging. When the cells or zebrafish were cultured without the analyte, the probe showed strong green fluorescence, which was quenched upon addition of the analyte, implying that **24** could detect exogenous ClO⁻. HeLa cells were also incubated with LPS to stimulate the endogenous production of ClO⁻, which was also detected (Scheme 3b).

Janczy-Cempa et al.[73] used the nitrocompounds **31a–b** as probes sensitive to nitroreductase, allowing in vivo hypoxia evaluation by imaging. The probes were synthesised by reacting the pyrazine **26** with NH-pyrazole (**27**) to form the N-hetarylpyrazole **28**, which then reacted with the appropriate nitroaryl derivative **29a–b** to yield the intermediates **30a–b**, which were finally subjected to a PIDA-mediated cyclization reaction (Scheme 3c). Probes **31a–b** showed λ_{abs} around 465 nm, λ_{em} around 541 nm, and very weak fluorescence as the nitro group quenched the process. The reduced fluorophores **32a–b** showed good photostability and responses against human

nitroreductase (NRD), even in the presence of interferents, and their fluorescence was not affected by molecular oxygen. To evaluate the bioimaging suitability of the probes, they were cultured with A2058 cells under normoxic and hypoxic conditions. Cells grown under normoxic conditions showed a slight fluorescence emission, possibly due to the activity of basal levels of NRD. However, when subjected to hypoxic conditions (less than 1% oxygen), the cells showed increased green emission, indicating a more significant reduction of probes **31a–b**.

Krishnaveni et al.[75] reported bisimine **35** as a probe for the in vivo detection of Zn²⁺ that was prepared by the condensation reaction of 5-bromosalicylaldehyde (**21b**) with hydrazine and then with 4-formylpyrazole **34** to produce the probe in a 98% yield. Probe **35** exhibited two λ_{abs} at 288 and 366 nm, a weak λ_{em} at 511 nm, a HOMO spread over the entire molecule, and a LUMO focused over the imine-bromophenol moiety. No fluorescence was observed for **35** due to the s-cis/s-trans isomerisation of the bisimine group (–CH=N–N=CH–). However, when **35** was complexed with Cd²⁺ or Zn²⁺, the HOMO was focused on the metal, while the LUMO remained similar; thus, the fluorescence in **35**-M was attributed to a metal-to-ligand charge transfer (MLCT). This probe could detect Zn²⁺ in HeLa cells and zebrafish embryos, exhibiting little toxicity. Zebrafish did not show fluorescence with **35** and without the analyte, while an intense yellow emission was observed under the exposition and internalisation with Zn²⁺ (Scheme 4a).

In the last example of 2021, Hosseinjani-Pirdehi et al.[76] obtained the tetrahydro-chromeno[2,3-c]pyrazole **39** by reacting 2 equivalents of pyrazolone **36** with formylated 1,3-biselectrophyle **37** to produce **38**, which ultimately suffered hydrazinolysis at **39** in a 40% yield (Scheme 4b). This probe was used for in vivo Cu²⁺ sensing and both **39** and **39**-Cu showed no displacements of λ_{abs} and λ_{em}, but the fluorescence was enhanced in **39**-Cu. For **39**, no fluorescence was observed due to the E/Z isomerisation of the hydrazone moiety, which was restricted once the metal had chelated, causing more rigidity in the molecule. This probe was used for bioimaging and the in vivo detection of Cu²⁺. Cells incubated solely with **39** showed no emission; however, the cells showed a greenish-yellow emission after Cu²⁺ was added to the culture. This result indicates that **39** had reasonable internalisation rates and could detect intracellular Cu²⁺. However, it is essential to note that **39** showed significant toxicity towards cells. Given this, **39** might not be the best tool for ion monitoring in living systems, but it could still be used for in vitro or ex vivo testing.
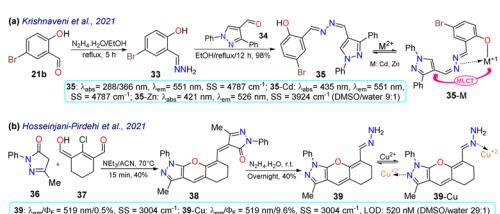
Scheme 4 Synthesis and photophysical data of (a) 35/35-M and (b) 39/39-Cu.

2.3. Probes reported in 2022

Liang *et al.*[37] obtained the 1,4-disubstituted pyrazoles **44** and **48** for the *in vivo* detection of c-Met, a protein highly expressed in solid tumours that is a strategic target for cancer diagnosis and detection. The synthesis started from the arylaldehyde **21c** or anhydride **45**, and it continued by incorporating a bromo-alkyl moiety that was then stirred with the pyrazolyl–boronic acid **41** to form the boronic esters **42** and **47**, which were subjected to a Suzuki–Miyaura reaction yielding **44** and **48**. Both dyes showed a photoinduced electron transfer (PET) process with fluorescence turn-off, in which the excited coumarin moiety transferred an electron to the receptor quinoline moiety; however, this process was inhibited upon binding to c-Met, turning on the emission of **44** and **48** (Schemes 5a and 5b). As for the bioimaging assays, both probes exhibited slight fluorescence in normal cells, which was related to basal levels of c-Met as this is a protein linked to several metabolic processes for almost any cell. In contrast, when the fluorophore was used with a c-Met overexpressing cell line, there was an apparent increase in the fluorescence, indicating that both probes could be used for detecting changes in the levels of c-Met. However, it must be considered that both dyes were highly toxic to at least two cell lines; thus, their application spectrum might not be as broad as expected.

Later, Bag *et al.*[77] synthesised the pyrazole derivative **52**, an excited-state intramolecular proton-transfer (ESIPT) active sensor for sensing Cu^{2+} in cells and plants. Their synthesis started from the 3-bromomethylsalicylaldehyde **21d** and the *NH*-pyrazole **49** to form the intermediate **50**; which was then reacted with sodium bisulfite and later with *o*-phenylenediamine **51** to yield the benzimidazole derivative **52**.[77] Unlike other sensors for metal cations analysed above, **52** was a turn-off sensor whose emission was quenched by adding Cu^{2+}. This dye exhibited a λ_{abs} at 326 nm and a λ_{em} at 474 nm with a Φ_F of 24%, whereas **52-Cu** showed a redshifted λ_{abs} at 379 nm with a λ_{em} that was not shifted but was dramatically decreased ($\Phi_F = 3\%$) due to an ESIPT process. In the excited state, the OH group of **52** formed intramolecular hydrogen bonds with pyridine-like nitrogen in pyrazole and benzimidazole rings, giving a strong blue emission; still, the fluorescence was quenched upon the

formation of **52-Cu** as the heteroatoms were occupied. Next, **52** was used for *in vivo* Cu^{2+} sensing, with MCF-7 cells, chickpeas, and Mung beans tested. For the cells, **52** showed almost no toxicity; while samples treated with **52** without Cu^{2+} showed strong blue emission inside the cells and the sprout of the beans, revealing that **52** could be well absorbed in mammal and plant cells. In contrast, when the samples were treated with **52** and Cu^{2+}, the fluorescence was quenched in cells and plants (Scheme 5c).

Roy *et al.*[78] obtained the pyrazolone **54** by reacting 3-methoxy-salicylaldehyde (**21e**) with the aminopyrazolone **53**. This probe showed three λ_{abs} at 230, 268, and 326 nm but was not fluorescent due to PET and ESIPT processes. However, complex **54-Al** showed a redshift to 404 nm. Upon the excitation of **54**, its aryloxyimine group transferred one electron to the adjacent enone moiety, and the molecular conformation allowed the intramolecular hydrogen bond formation. Notably, the PET and ESIPT processes were not viable after forming **54-Al** as the heteroatom donors were occupied in chelating the Al^{3+} (Scheme 6a). Likewise, **54** was used for intracellular Al^{3+} sensing by bioimaging, with an absence of emission observed for cells treated with Al^{3+}, but once the dye was added, a strong green fluorescence was seen. Nevertheless, care must be taken when using this probe as it was confirmed through utilising an acridine orange/ethidium bromide co-staining assay that the **54-Al** complex may interact with single-stranded DNA, which could affect the cell cycle and lead to cell death *via* apoptosis.

Finally, Kuznetsov *et al.*[79] prepared the phosphorescent probe **59** by a Suzuki coupling of the arylboronic acid **55** with the heteroaryl chloride **56**, yielding the tridentate ligand **57**, which then reacted with the Eu(III) complex **58**, delivering **59**. This probe showed two λ_{abs} at 344 and 391 nm with a λ_{em} at 612 nm, typical for Eu(III) complexes (Scheme 6b). As NIR radiation is minor phototoxic and more penetrating than visible radiation, these results suggest the probe would not cause cellular photodamage and would offer deep tissue penetration. By testing the temperature effect on the luminescence of **59**, it was found that raising the temperature reduced the lifetime of its emission, indicating its high sensitivity to temperature changes. Nanoparticles **59-NPs** with a superficial positive charge were also prepared as their target is the mitochondrion, whose membrane is anionic. Still, **59-NPs** were found in endosomes, lysosomes, or similar parts, not in the mitochondria. Moreover, phosphorescence lifetime imaging microscopy (PLIM) assays were used with uncharged **59-NPs** for sensing
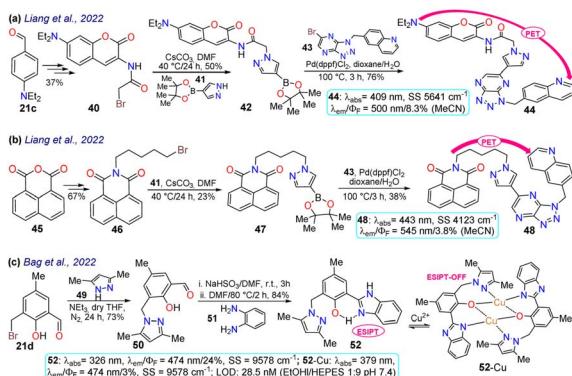
Scheme 5 Synthesis and photophysical data of (a) **44**, (b) **48**, and (c) **52/52-Cu**.
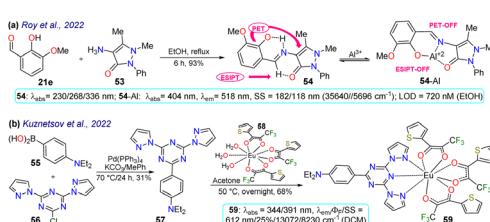
Scheme 6 Synthesis and photophysical data of probes (a) **54/54-Al** and (b) **59**.

cellular temperature. The images showed a general typical temperature in cells, although some colder spots could also be seen. However, these results were good enough to indicate that the probe is suitable and viable for intracellular temperature review. The same behaviour was found for modified **59**-NPs, indicating that the cationic surface did not affect its sensing properties.

2.4. Probes reported in 2023

Krishnan *et al.*[80] synthesised pyrazolo[4,3-*b*]pyridine **62** in an 85% yield through a Povarouv reaction of 5-aminopyrazole **60** with the arylaldehyde **61** and then used this probe for the detection of BF_3 in *E. coli* and HeLa cells. Probe **62** displayed an absorption band at 336 nm and an emission band at 440 nm, which were then redshifted in the presence of BF_3 – at 368 and 473 nm, respectively. Upon gradual BF_3 addition, the absorption band of probe **62** decreased while the fluorescence band increased, increasing the quantum yield from 35% to 65% due to ICT from the alkoxy group to the boron atom. Probe **62** was tested in the presence of *E. coli* cells, with blue fluorescence observed once the bacterial culture was incubated with BF_3. Also, 3-(4,5-dimethylthiazol-2-yl)-2,5-diphenyltetrazolium bromide (MTT) assays were performed, offering green fluorescence, which indicates that the intracellular uptake of BF_3 resulted in the complexation in the intracellular region (Scheme 7a).

In another work, Shi *et al.*[81] prepared 3-(coumarin-3-yl) pyrazole **65** by two steps in an 87% yield, implying a cyclo-condensation reaction of the β-diketone **63** with hydrazine, followed by a sulfonylation reaction with 2,4-dini-trobenzenesulfonyl chloride (**64**). This probe exhibited a λ_{abs} at 425 nm and a λ_{em} at 500 nm without a shift in these wavelengths in the presence of H_2S. Nevertheless, upon analyte addition, the solution changed its colour, and the Φ_F was enhanced from 5% to 27% as a PET-OFF process was activated once the sulfonyl group was cleaved in **64** by H_2S. Competitive assays were performed with varied cations, anions, and some amino acids, and it was found that the reaction with H_2S was unperturbed by the presence of other analytes and lasted 3 min. Still, with other analytes like cysteine, the reaction took 30 min or longer.
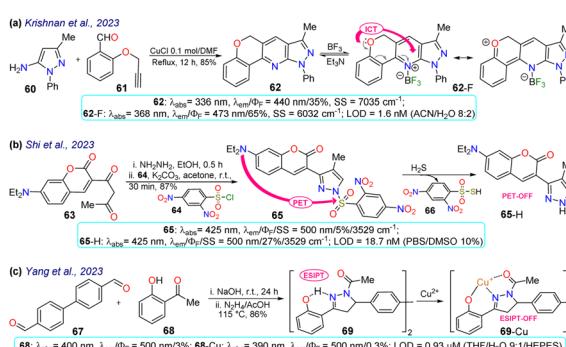
Ultimately, the authors investigated the recognition of exogenous and endogenous H_2S in MCF-7 cells, which were incubated with the analyte and a fluorescence turn-on of the cells was observed with an LOD of 18.7 nM (Scheme 7b).

Yang *et al.*[82] synthesised the bispyrazoline **69** in an 86% yield through a condensation reaction of 4,4′-diformylbiphenyl (**67**) with 2-hydroxyacetophenone **68** followed by a cyclisation reaction with hydrazine. Probe **69** exhibited a λ_{abs} at 400 nm, shifted to 390 nm in the presence of Cu^{2+}, and a λ_{em} at 500 nm. In the presence of the analyte, the fluorescence decreased, with Φ_F going from 3% to 0.3% due to an interrupted ESIPT process. Biological assays were performed on HeLa cells with **69** and **69**-Cu, evidencing that these cells had blue emission with good permeability in the presence of **69**, and then by adding Cu^{2+} to the system, the fluorescence signal weakened, making it suitable for the detection of intracellular copper ions (Scheme 7c).

Two examples of pyrazoles were reported in 2023 that do not present an approach to bioimaging but focus on the design of fluorophores, as discussed below. First, Wei *et al.*[83] obtained **72** by condensing 3-pyrazolylhydrazide **70** with salicylaldehyde **71**. This probe showed two λ_{abs} at 309 and 374 nm, which were shifted to 281 and 406 nm upon the addition of Ga^{3+} ions. Likewise, weak fluorescence was observed ($\Phi_F = 0.2\%$), which was increased ($\Phi_F = 57\%$) in the presence of the analyte, obtaining an LOD of 12.1 mM. The almost no fluorescence of **72** was due to a PET-OFF process in the complex **72**-Ga. The authors studied the effect of the diethylamino group in **72**, evidencing the necessity of this group for the photophysical properties (Scheme 8a). Second, Patil *et al.*[84] synthesised the imine **74** in an 80% yield using the reaction of 4-amino-antipyrine (**72**) with 2,5-dihydroxyacetophenone (**73**). This dye exhibits two λ_{abs} at 326 and 364 nm, but in the presence of Cu^{2+}, the band at 364 nm was shifted to 425 nm (Scheme 8b). Upon increasing the concentration of Cu^{2+}, a progressive rise and decrease in the peaks at 425 and 364 nm, respectively, was observed, which evidenced the formation of the complex **74**-Cu, which favoured a ligand-to-metal charge transfer (LMCT). An emission peak at 465 nm was evidenced for **74** and **74**-Cu, with fluorescence enhancement in the presence of Cu^{2+} due to a chelation-enhanced fluorescence process (CHEF).

2.5. Probes reported in 2024

Rasin *et al.*[85] synthesised the fused pyrazole **78** by the cyclisation reaction of the 1,3-biselectrophyle **76** with the

Scheme 7 Synthesis and optical data of probes based on (a) pyrazolopyridine **62**/**62**-F, (b) 3-(coumarin-3-yl)pyrazole **65**/**65**-H, and (c) pyrazoline **69**/**69**-Cu.
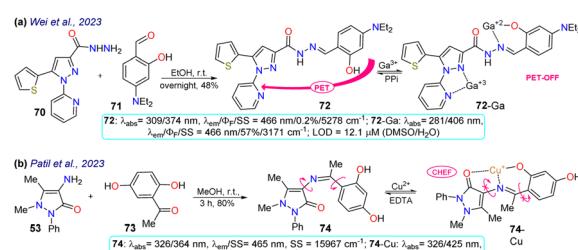

Scheme 8 Synthesis and optical data of (a) **72**/**72**-Ga and (b) **74**/**74**-Cu.

thiosemicarbazide **77**. Probe **78** exhibited two absorption bands at 325 nm and 372 nm, and upon the addition of fluoride ions, a new band emerged around 430 nm, indicating the formation of **78**-F; **78** displayed a λ_{em} at 476 nm that was shifted to 492 nm for **78**-F with an increase in the Φ_F from 38% to 64%. Complex **78**-F demonstrated a fluorescence enhancement compared to **78**, which linked the relaxation from the stimulated state to the PET process. The authors investigated the detection of the anion on T24 living cells, and blue fluorescence was observed once the cells were treated with the sensor and fluoride ions, indicating that **78** could detect the anion on the cell's cytoplasm (Scheme 9a).

Li *et al.*[86] designed probe **83** to detect aqueous acid, which was obtained using the condensation reaction of the bicyclic ketone **79** with ethyl isonicotinate **80** to form the β-diketone **81**, which finally cyclocondensed with phenylhydrazine (**82**). Probe **83** exhibited an absorption band at 375 nm, which was gradually diminished with the increase in the medium's acidity, and a new peak emerged at 438 nm. Likewise, an emission band at 487 nm was observed that decreased as the acidity increased, while a new peak at 585 nm emerged. These spectral changes were caused by protonation of the pyridine ring generating an ICT effect that led to the redshift of the spectrum. The authors conducted fluorescent bioimage studies, which indicated that **83** exhibited low cytotoxicity, making the probe well suited for monitoring pH alterations of zebrafishes as they show a strong fluorescence in acidic media (Scheme 9b).

Liu *et al.*[87] obtained the pyrazole **87** by the cyclocondensation reaction of malonaldehyde (**86**) with the hetarylhydrazine **85**, which was obtained *via* diazonium salts from the hetarylamine **84** (Scheme 9c). The 4-trifluoromethylquinoline group of **85** was the Golgi-target, and the hydrazine group was the recognition site. This probe exhibited an emission band at 424 nm but showed no fluorescence, due to the PET process generated by the presence of the amino group. However, once the probe reacted with **86**, forming **87**, the electron-donating capacity of the amino group was affected, offering both PET-OFF and ICT phenomena with a redshift in the emission spectra and an enhanced fluorescence. The MTT method was used with **87**, and low cytotoxicity was found. Then, the ability of **85** to Golgi apparatus was proved by labelling HeLa cells and red staining the Golgi apparatus, with blue emission detected, indicating the

Scheme 9 Synthesis and photophysical data of fluorophores (a) **78**/**78**-F, (b) **83**/**83**-H, and (c) **85**/**87**.
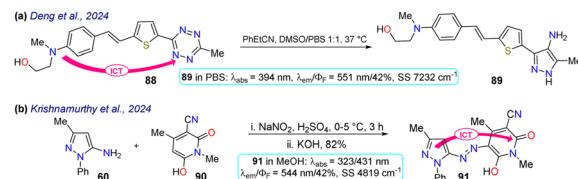
**Scheme 10** Synthesis and photophysical data of the probes (a) **89** and (b) **91**.

excellent targeting of the probe with the desired target, with an LOD of 71 nM.

Deng and colleagues prepared the probe **89** using the reaction of tetrazine **88** with phenyl-propanenitrile, a type of [4 + 1] cycloaddition that is an alternative to the inverse electron-demanding Diels–Alder reaction that has gained attention in protein labelling, and drug delivery and thanks to its biocompatibility, rapid kinetics, and effective payload release (Scheme 10a).[88] Probe **89** exhibited absorption and emission bands at 394 and 551 nm, respectively, with a Φ_F of 42% in PBS buffer, probably giving an ICT-OFF process that initially occurs from the dialkylamino group to the π-deficient tetrazine ring. This probe was studied with live 193T-cell labelling on intracellular targets (nucleus proteins and mitochondria). Vivid mitochondria stains and orthogonal labelling were observed in the membrane, suggesting probe **89** is suitable for labelling bioimages.

Finally, Krishnamurthy *et al.*[89] synthesised probe **91** in an 82% yield starting from the 5-aminopyrazole **60**, which underwent diazotization followed by a coupling reaction with the cyanomethyl-pyridone **90**. Probe **91** exhibited two absorption peaks at 323 nm and 431 nm and an emission peak at 544 nm with a Φ_F of 42% in methanol, which helped stabilise the hydrazo tautomer **91**. In solvents such as MeOH, DMSO, and DMF, the hydrazo form was stabilised generating a redshift on the absorption peaks, while in MeCN, DCM, and chloroform the azo form was stabilised generating a blue-shift on the spectra. An ICT process was responsible for the fluorescence of probe **91**. This property was used for bioimaging in HeLa cells, with a strong green fluorescence observed, and was studied for the electrochemical detection of dopamine, demonstrating an LOD of 0.81 mM (Scheme 10b).

3 Conclusions

In summary, diverse synthetic transformations implying fluorescent pyrazoles have been reported, some by ring construction and others using functionalisation or derivatisation strategies, usually by classical reactions and reaction conditions that are easily reproducible. In this manner, novel functional pyrazoles with relevant applications have been obtained, with some examples finding use in bioimaging applications. These fluorescent dyes have proven to offer exceptional results in general cell staining and the detection of in-cell conditions, like temperature or hypoxia. The compounds herein discussed include further structural motifs, from additional heterocyclic, pyrazolines, or fluorescent groups to complexes with metal ions,
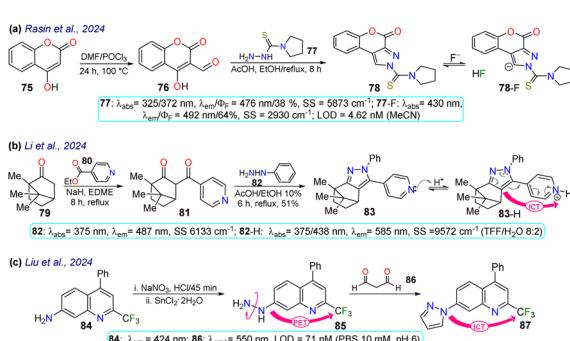
for which different synthetic approaches are needed. For the evaluated systems, ICT, PET, and MLCT are the most prevalent photophysical phenomena that govern the fluorescence of the probes, which, upon reacting with the target (like metal ions, small molecules, or enzymes), is either enhanced or 'turned-off', leading to observable changes in the fluorescence that allow the sensing of the different targets, which in turn is what leads to pyrazole derivatives having so many applications. Various molecular architectures of pyrazoles-based compounds have been used in bioimaging applications, in which the incorporation of EDGs or highly conjugated substituents is the main constant in the probe design. Also, the probes must be functionalised with appropriate receptors (*e.g.* ion receptors, lipophilic fragments, or hydrogen bond mediators) so that they can perform their work in different environments. Notably, although there are many published articles on fluorescent probes for bioimaging applications based on small molecules, several of these works did not carry out an appropriate photophysical study for the respective development; as a result, a good look at this review could pointedly improve this issue.

Data availability

This review manuscript presents original work submitted for publication only in RSC Advances. The authors have no conflicts of interest to report with this submission, and they have all seen, revised, and approved this paper, which details the chemistry and properties of fluorescent probes based on pyrazole/pyrazoline derivatives with a focus on bioimaging applications.

Author contributions

The individuals listed as authors have contributed to developing this manuscript, and no other person was involved. The authors' contributions included M.-C. R. and S. M.-H. ran the article's research and analyses and the original draft composition, and J. P. conducted the composition of the original draft, edition, conceptualization, supervision, and sources. All authors have read and agreed to the published version of this manuscript.

Conflicts of interest

The authors declare no competing financial interest.

Acknowledgements

Notes and references

1 Z. Guo, S. Park, J. Yoon and I. Shin, Recent progress in the development of near-infrared fluorescent probes for bioimaging applications, *Chem. Soc. Rev.*, 2014, **43**, 16–29.

2 M. Won, M. Li, H. S. Kim, P. Liu, S. Koo, S. Son, J. H. Seo and J. S. Kim, Visible to mid IR: A library of multispectral diagnostic imaging, *Coord. Chem. Rev.*, 2021, **426**, 213608.

3 T. Terai and T. Nagano, Fluorescent probes for bioimaging applications, *Curr. Opin. Cell Biol.*, 2008, **12**, 515–521.

4 T. Terai and T. Nagano, Small-molecule fluorophores and fluorescent probes for bioimaging, *Pflügers Arch.*, 2013, **465**, 347–359.

5 B. A. D. Neto, J. E. P. Sorto, A. A. M. Lapis and F. Machado, Functional chromophores synthesized *via* multicomponent Reactions: A review on their use as cell-imaging probes, *Methods*, 2023, **220**, 142–157.

6 J. Milczarek, R. Pawlowska, R. Zurawinski, B. Lukasik, L. E. Garner and A. Chworos, Fluorescence and confocal imaging of mammalian cells using conjugated oligoelectrolytes with phenylenevinylene core, *J. Photochem. Photobiol., B*, 2017, **170**, 40–48.

7 V. P. De Souza, V. Vendrusculo, A. M. Morás, L. Steffens, F. S. Santos, D. J. Moura, F. S. Rodembusch and D. Russowsky, Synthesis and photophysical study of new fluorescent proton transfer dihydropyrimidinone hybrids as potential candidates for molecular probes, *New J. Chem.*, 2017, **41**, 15305–15311.

8 Y. Li, Q. Chen, X. Pan, W. Lu and J. Zhang, Development and Challenge of Fluorescent Probes for Bioimaging Applications: From Visualization to Diagnosis, *Top. Curr. Chem.*, 2022, **380**, 22.

9 D. Pirone, J. Lim, F. Merola, L. Miccio, M. Mugnano, V. Bianco, F. Cimmino, F. Visconte, A. Montella, M. Capasso, A. Iolascon, P. Memmolo, D. Psaltis and P. Ferraro, Stain-free identification of cell nuclei using tomographic phase microscopy in flow cytometry, *Nat. Photonics*, 2022, **16**, 851–859.

10 R. R. Mayank, A. Singh, N. Garg, N. Kaur and N. Singh, Mitochondria- and nucleolus-targeted copper(i) complexes with pyrazole-linked triphenylphosphine moieties for live cell imaging, *Analyst*, 2020, **145**, 83–90.

11 M. Gao, H. Su, S. Li, Y. Lin, X. Ling, A. Qin and B. Z. Tang, An easily accessible aggregation-induced emission probe for lipid droplet-specific imaging and movement tracking, *Chem. Commun.*, 2017, **53**, 921–924.

12 A. Reicher, J. Reiniš, M. Ciobanu, P. Růžička, M. Malik, M. Siklos, V. Kartysh, T. Tomek, A. Koren, A. F. Rendeiro and S. Kubicek, Pooled multicolour tagging for visualizing subcellular protein dynamics, *Nat. Cell Biol.*, 2024, **26**, 745–756.

13 M. O. Rodrigues, M. N. Eberlin and B. A. D. Neto, How and Why to Investigate Multicomponent Reactions Mechanisms? A Critical Review, *Chem. Rec.*, 2021, **21**, 2762–2781.

14 S. Das, H. K. Indurthi, P. Asati and D. K. Sharma, Small Molecule Fluorescent Probes for Sensing and Bioimaging of Nitroreductase, *ChemistrySelect*, 2022, **7**, e202102895.

15 J. T. Hou, K. K. Yu, K. Sunwoo, W. Y. Kim, S. Koo, J. Wang, W. X. Ren, S. Wang, X. Q. Yu and J. S. Kim, Fluorescent Imaging of Reactive Oxygen and Nitrogen Species Associated with Pathophysiological Processes, *Chem*, 2020, **6**, 832–866.

16 L. C. Murfin, M. Weber, S. J. Park, W. T. Kim, C. M. Lopez-Alled, C. L. McMullin, F. Pradaux-Caggiano, C. L. Lyall, G. Kociok-Köhn, J. Wenk, S. D. Bull, J. Yoon, H. M. Kim, T. D. James and S. E. Lewis, Azulene-Derived Fluorescent Probe for Bioimaging: Detection of Reactive Oxygen and Nitrogen Species by Two-Photon Microscopy, *J. Am. Chem. Soc.*, 2019, **141**, 19389–19396.

17 A. Tigreros and J. Portilla, Fluorescent Pyrazole Derivatives: An Attractive Scaffold for Biological Imaging Applications, *Curr. Chin. Sci.*, 2021, **1**, 197–206.

18 H. Chen, F. Ding, Z. Zhou, X. He and J. Shen, FRET-based sensor for visualizing pH variation with colorimetric/ratiometric strategy and application for bioimaging in living cells, bacteria and zebrafish, *Analyst*, 2020, **145**, 4283–4294.

19 S. Gond, P. Yadav, B. S. Chauhan, S. Srikrishna and V. P. Singh, Development of an 'OFF-ON-OFF' colorimetric and fluorometric pH sensor for the study of physiological pH and its bioimaging application, *J. Mol. Struct.*, 2022, **1252**, 132147.

20 X.-L. Xue, Y. Wang, S. Chen, K.-P. Wang, S.-Y. Niu, Q.-S. Zong, Y. Jiang and Z.-Q. Hu, Monitoring intracellular pH using a hemicyanine-based ratiometric fluorescent probe, *Spectrochim. Acta, Part A*, 2023, **284**, 121778.

21 N. Bauer, I. Maisuls, A. Pereira da Graça, D. Reinhardt, R. Erapaneedi, N. Kirschnick, M. Schäfers, C. Grashoff, K. Landfester, D. Vestweber, C. A. Strassert and F. Kiefer, Genetically encoded dual fluorophore reporters for graded oxygen-sensing in light microscopy, *Biosens. Bioelectron.*, 2023, **221**, 114917.

22 V. Mirabello, F. Cortezon-Tamarit and S. I. Pascu, Oxygen Sensing, Hypoxia Tracing and in Vivo Imaging with Functional Metalloprobes for the Early Detection of Non-communicable Diseases, *Front. Chem.*, 2018, **6**, 00027.

23 D. Chen, W. Wang, Q. Zhu, Q. Wang, D. Quan, Y. Zeng, K. Li, Y. Zhou, C. Liu, W. Zhan and Y. Zhan, In vivo real-time monitoring of the development of hypoxia and angiogenesis in cervical cancer, *J. Chem. Eng*, 2023, **473**, 145498.

24 P. Feng, H. Zhang, Q. Deng, W. Liu, L. Yang, G. Li, G. Chen, L. Du, B. Ke and M. Li, Real-Time Bioluminescence Imaging of Nitroreductase in Mouse Model, *Anal. Chem.*, 2016, **88**, 5610–5614.

25 Q. Yang, S. Wang, D. Li, J. Yuan, J. Xu and S. Shao, A mitochondria-targeting nitroreductase fluorescent probe with large Stokes shift and long-wavelength emission for imaging hypoxic status in tumor cells, *Anal. Chim. Acta*, 2020, **1103**, 202–211.

26 W. Wanas, S. A. Abd El-Kaream, S. Ebrahim, M. Soliman and M. Karim, Cancer bioimaging using dual mode luminescence of graphene/FA-ZnO nanocomposite based on novel green technique, *Sci. Rep.*, 2023, **13**, 27.

27 B. Brennecke, Q. Wang, Q. Zhang, H. Y. Hu and M. Nazaré, An Activatable Lanthanide Luminescent Probe for Time-Gated Detection of Nitroreductase in Live Bacteria, *Angew. Chem., Int. Ed.*, 2020, **59**, 8512–8516.

28 Q. Yang, Y. Wen, A. Zhong, J. Xu and S. Shao, An HBT-based fluorescent probe for nitroreductase determination and its application in: Escherichia coli cell imaging, *New J. Chem.*, 2020, **44**, 16265–16268.

29 H. Jiang, Z. Cao, Y. Liu, R. Liu, Y. Zhou and J. Liu, Bacteria-Based Living Probes: Preparation and the Applications in Bioimaging and Diagnosis, *Adv. Sci.*, 2024, **11**, 2306480.

30 Y. Fan, M. Lu, X. A. Yu, M. He, Y. Zhang, X. N. Ma, J. Kou, B. Y. Yu and J. Tian, Targeted Myocardial Hypoxia Imaging Using a Nitroreductase-Activatable Near-Infrared Fluorescent Nanoprobe, *Anal. Chem.*, 2019, **91**, 6585–6592.

31 J. Zheng, Y. Shen, Z. Xu, Z. Yuan, Y. He, C. Wei, M. Er, J. Yin and H. Chen, Near-infrared off-on fluorescence probe activated by NTR for *in vivo* hypoxia imaging, *Biosens. Bioelectron.*, 2018, **119**, 141–148.

32 X. Han, R. Wang, X. Song, F. Yu, C. Lv and L. Chen, A mitochondrial-targeting near-infrared fluorescent probe for bioimaging and evaluating endogenous superoxide anion changes during ischemia/reperfusion injury, *Biomaterials*, 2018, **156**, 134–146.

33 J. Qian and B. Z. Tang, AIE Luminogens for Bioimaging and Theranostics: From Organelles to Animals, *Chem*, 2017, **3**, 56–91.

34 C. Pigot, D. Brunel and F. Dumur, Indane-1,3-Dione: From Synthetic Strategies to Applications, *Molecules*, 2022, **27**, 5976.

35 S. M. Bentzen, Theragnostic imaging for radiation oncology: dose-painting by numbers, *Lancet Oncol.*, 2005, **6**, 112–117.

36 M. J. Mantilla, C. E. Cabrera Díaz, G. Ariza-Aranguren, H. de Cock, J. B. Helms, S. Restrepo, E. Jiménez and A. M. Celis Ramírez, Back to the Basics: Two Approaches for the Identification and Extraction of Lipid Droplets from *Malassezia pachydermatis* CBS1879 and *Malassezia globosa* CBS7966, *Curr. Protoc.*, 2021, **1**, e122.

37 D. Liang, C. Yu, X. Qin, X. Yang, X. Dong, M. Hu, L. Du and M. Li, Discovery of small-molecule fluorescent probes for C-Met, *Eur. J. Med. Chem.*, 2022, **230**, 114114.

38 A. Tigreros, M. Macías and J. Portilla, Structural, Photophysical, and Water Sensing Properties of Pyrazolo [1,5-a]pyrimidine-Triphenylamine Hybrid Systems, *ChemPhotoChem*, 2022, **2022**, e202200133.

39 D. Cao, Z. Liu, P. Verwilst, S. Koo, P. Jangjili, J. S. Kim and W. Lin, Coumarin-Based Small-Molecule Fluorescent Chemosensors, *Chem. Rev.*, 2019, **119**, 10403–10519.

40 J. Xie, L. Wang, X. Su and J. Rodrigues, Coumarin-based Fluorescent Probes for Bioimaging: Recent Applications and Developments, *Curr. Org. Chem.*, 2021, **25**, 2142–2154.

41 R. J. Grams, W. L. Santos, I. R. Scorei, A. Abad-García, C. A. Rosenblum, A. Bita, H. Cerecetto, C. Viñas and M. A. Soriano-Ursúa, The Rise of Boron-Containing Compounds: Advancements in Synthesis, Medicinal

Chemistry, and Emerging Pharmacology, *Chem. Rev.*, 2024, **124**, 2441–2511.

42 S. Das, S. Dey, S. Patra, A. Bera, T. Ghosh, B. Prasad, K. D. Sayala, K. Maji, A. Bedi and S. Debnath, BODIPY-Based Molecules for Biomedical Applications, *Biomolecules*, 2023, **13**, 1723.

43 M. C. Rios, N. F. Bravo, C. C. Sanchez and J. Portilla, Chemosensors based on N-heterocyclic dyes: Advances in sensing highly toxic ions such as CN- and Hg2+, *RSC Adv.*, 2021, **11**, 34206–34234.

44 J. T. Sarmiento and J. Portilla, Current Advances in Diazoles-based Chemosensors for CN- and FDetection, *Curr. Org. Synth.*, 2023, **20**, 77–95.

45 J. Zhang, X. Chai, X.-P. He, H.-J. Kim, J. Yoon and H. Tian, Fluorogenic probes for disease-relevant enzymes, *Chem. Soc. Rev.*, 2019, **48**, 683–722.

46 Y. Yang, Q. Zhao, W. Feng and F. Li, Luminescent Chemodosimeters for Bioimaging, *Chem. Rev.*, 2013, **113**, 192–270.

47 C. L. Fleming, P. A. Sandoz, T. Inghardt, B. Önfelt, M. Grøtli and J. Andréasson, A Fluorescent Kinase Inhibitor that Exhibits Diagnostic Changes in Emission upon Binding, *Angew. Chem., Int. Ed.*, 2019, **58**, 15000–15004.

48 L. Türker and S. Variş, A review of polycyclic aromatic energetic materials, *Polycyclic Aromat. Compd.*, 2009, **29**, 228–266.

49 M. Stępień, E. Gońka, M. Żyła and N. Sprutta, Heterocyclic Nanographenes and Other Polycyclic Heteroaromatic Compounds: Synthetic Routes, Properties, and Applications, *Chem. Rev.*, 2017, **117**, 3479–3716.

50 H. M. Kim and B. R. Cho, Small-Molecule Two-Photon Probes for Bioimaging Applications, *Chem. Rev.*, 2015, **115**, 5014–5055.

51 A. Loudet and K. Burgess, BODIPY Dyes and Their Derivatives: Syntheses and Spectroscopic Properties, *Chem. Rev.*, 2007, **107**, 4891–4932.

52 M. O. Senge, N. N. Sergeeva and K. J. Hale, Classic highlights in porphyrin and porphyrinoid total synthesis and biosynthesis, *Chem. Soc. Rev.*, 2021, **50**, 4730–4789.

53 J. Hwang, T. S. Reddy, H. Moon, H. D. Lee and M.-S. Choi, Cyanide detecting porphyrin fluorescent sensors: Effects of electron-donating/withdrawing substituents, *Dyes Pigm.*, 2023, **215**, 111243.

54 A. L. Pang, A. Arsad and M. Ahmadipour, Synthesis and factor affecting on the conductivity of polypyrrole: a short review, *Polym. Adv. Technol.*, 2021, **32**, 1428–1454.

55 F.-Z. Li, J.-F. Yin and G.-C. Kuang, BODIPY-based supramolecules: Construction, properties and functions, *Coord. Chem. Rev.*, 2021, **448**, 214157.

56 D. Kim, D. Ma, M. Kim, Y. Jung, N. H. Kim, C. Lee, S. W. Cho, S. Park, Y. Huh, J. Jung and K. H. Ahn, Fluorescent Labeling of Protein Using Blue-Emitting 8-Amino-BODIPY Derivatives, *J. Fluoresc.*, 2017, **27**, 2231–2238.

57 M. L. S. O. Lima, C. B. Braga, T. B. Becher, M. Odriozola-Gimeno, M. Torrent-Sucarrat, I. Rivilla, F. P. Cossío, A. J. Marsaioli and C. Ornelas, Fluorescent Imidazo[1,2-a]pyrimidine Compounds as Biocompatible Organic Photosensitizers that Generate Singlet Oxygen: A Potential Tool for Phototheranostics, *Chem.–Eur. J.*, 2021, **27**, 6213–6222.

58 A. Kolbus, T. Uchacz, A. Danel, K. Gałczyńska, P. Moskwa and P. Kolek, Fluorescent Sensor Based on 1H-Pyrazolo [3,4-b]quinoline Derivative for Detecting Zn2+ Cations, *Molecules*, 2024, **29**, 823.

59 J. Orrego-Hernández, C. Lizarazo, J. Cobo and J. Portilla, Pyrazolo-fused 4-azafluorenones as key reagents for the synthesis of fluorescent dicyanovinylidene-substituted derivatives, *RSC Adv.*, 2019, **9**, 27318–27323.

60 K. Saravana Mani, R. Rajamanikandan, G. Ravikumar, B. Vijaya Pandiyan, P. Kolandaivel, M. Ilanchelian and S. P. Rajendran, Highly Sensitive Coumarin–Pyrazolone Probe for the Detection of Cr $^{3+}$ and the Application in Living Cells, *ACS Omega*, 2018, **3**, 17212–17219.

61 S. B. Subramaniyan, S. B. Annes, M. Yuvasri, K. Nivedha, S. Ramesh and V. Anbazhagan, 1,3,5-Triphenylpyrazoline Based Fluorescent Probe for Selective Sensing and Imaging of Glutathione in Live Cell under Oxidative Stress, *ChemistrySelect*, 2020, **5**, 515–521.

62 A. Tigreros and J. Portilla, Recent progress in chemosensors based on pyrazole derivatives, *RSC Adv.*, 2020, **10**, 19693–19712.

63 M.-C. Ríos and J. Portilla, Recent Advances in Synthesis and Properties of Pyrazoles, *Chemistry*, 2022, **4**, 940–968.

64 J. Portilla, Current Advances in Synthesis of Pyrazole Derivatives: An Approach Toward Energetic Materials, *J. Heterocycl. Chem.*, 2024, **61**(12), 2026–2039.

65 J. Orrego-Hernández, J. Cobo and J. Portilla, Synthesis, Photophysical Properties, and Metal-Ion Recognition Studies of Fluoroionophores Based on 1-(2-Pyridyl)-4-Styrylpyrazoles, *ACS Omega*, 2019, **4**, 16689–16700.

66 M. U. Sarveswari S., A review on pyrazole moieties as organic chemosensors in the detection of cations and anions, *Inorg. Chim. Acta*, 2024, **569**, 122118.

67 Y. Zhang, X. Zheng, L. Zhang, Z. Yang, L. Chen, L. Wang, S. Liu and Z. Xie, Red fluorescent pyrazoline-BODIPY nanoparticles for ultrafast and long-term bioimaging, *Org. Biomol. Chem.*, 2020, **18**, 707–714.

68 X. B. Wang, H. J. Li, Z. Chi, X. Zeng, L. J. Wang, Y. F. Cheng and Y. C. Wu, A novel mitochondrial targeting fluorescent probe for ratiometric imaging SO2 derivatives in living cells, *J. Photochem. Photobiol., A*, 2020, **390**, 112339.

69 L. R. V. Favarin, G. B. Laranjeira, C. F. A. Teixeira, H. Silva, A. C. Micheletti, L. Pizzuti, A. Machulek Júnior, A. R. L. Caires, V. M. Deflon, R. B. P. Pesci, C. N. L. Rocha, J. R. Correa, L. M. C. Pinto and G. A. Casagrande, Harvesting greenish blue luminescence in gold(i) complexes and their application as promising bioactive molecules and cellular bioimaging agents, *New J. Chem.*, 2020, **44**, 6862–6871.

70 A. Alizadeh, B. Farajpour, S. S. Mohammadi, M. Sedghi, H. Naderi-Manesh, C. Janiak and T. Knedel, Design and Synthesis of Coumarin-Based Pyrazolopyridines as Biocompatible Fluorescence Dyes for Live-Cell Imaging, *ChemistrySelect*, 2020, **5**, 9362–9369.

71 X. Wang, L. Wang, L. Xie, Z. Xie, L. Li, D. Bui, T. Yin, S. Gao and M. Hu, Design and Synthesis of a Novel NIR Celecoxib-Based Fluorescent Probe for Cyclooxygenase-2 Targeted Bioimaging in Tumor Cells, *Molecules*, 2020, **25**, 4037.

72 X. He, X. Cao, X. Tian and Y. Bai, A simple fluorescent probe for glutathione detection and its bioimaging application in living cells, *Microchem. J.*, 2021, **166**, 106135.

73 E. Janczy-Cempa, O. Mazuryk, D. Sirbu, N. Chopin, M. Żarnik, M. Zastawna, C. Colas, M. A. Hiebel, F. Suzenet and M. Brindell, Nitro-Pyrazinotriazapentalene scaffolds–nitroreductase quantification and *in vitro* fluorescence imaging of hypoxia, *Sens. Actuators, B*, 2021, **346**, 130504.

74 Y. Huang, Y. Zhang, F. Huo and C. Yin, An innovative hypochlorite-sensing scaffold and its imaging application in vivo, *Dyes Pigm.*, 2021, **191**, 109378.

75 K. Krishnaveni, S. Murugesan and A. Siva, Fluorimetric and colorimetric detection of multianalytes Zn2+/Cd2+/F− ions *via* 5-bromosalicyl hydrazone appended pyrazole receptor; live cell imaging analysis in HeLa cells and zebra fish embryos, *Inorg. Chem. Commun.*, 2021, **132**, 108843.

76 H. Hosseinjani-Pirdehi, N. O. A. Mahmoodi and A. Taheri, Selective Cu2+ detection by a novel fluorescence hydrazone – Base probe in aqueous media, *J. Photochem. Photobiol., A*, 2021, **421**, 113524.

77 R. Bag, Y. Sikdar, S. Sahu, C. Das Mukhopadhyay, M. G. B. Drew and S. Goswami, Benzimidazole based ESIPT active chemosensors enable nano–molar detection of Cu2+ in 90% aqueous solution, MCF–7 cells, and plants, *J. Photochem. Photobiol., A*, 2022, **431**, 114006.

78 S. Roy, S. Kundu, S. Saha, K. Muddukrishnaiah, R. Pramanik and B. Biswas, Visible light-triggered pyrazole-functionalized reversible ionophore for selective monitoring of aluminium (III) ion, *Appl. Organomet. Chem.*, 2022, **36**, e6865.

79 K. M. Kuznetsov, V. A. Baigildin, A. I. Solomatina, E. E. Galenko, A. F. Khlebnikov, V. V. Sokolov, S. P. Tunik and J. R. Shakirova, Polymeric Nanoparticles with Embedded Eu(III) Complexes as Molecular Probes for Temperature Sensing, *Molecules*, 2022, **27**, 8813.

80 U. Krishnan, S. Manickam and S. K. Iyer, BF3 detection by pyrazolo-pyridine based fluorescent probe and applications in bioimaging and paper strip analysis, *J. Mol. Liq.*, 2023, **385**, 122413.

81 G. J. Shi, Y. D. Wang, Z. X. Yu, Q. Zhang, S. Chen, L. Z. Xu, K. P. Wang and Z. Q. Hu, The coumarin-pyrazole dye for detection of hydrogen sulfide in cells, *Spectrochim. Acta, Part A*, 2023, **285**, 121898.

82 Y. S. Yang, F. N. Wang, Y. P. Zhang, F. Yang and J. J. Xue, Novel Bis-pyrazoline Fluorescent Probe for Cu2+ and Fe3+ Detection and Application in Cell Imaging, *J. Fluoresc.*, 2024, **34**, 159–167.

83 K. Wei, B. Zhang, Y. Liu, M. Kang, P. Liu, X. Yang, M. Pei and G. Zhang, Comparison of two pyrazole derived "turn on" fluorescent probes for the recognition of Ga3+, *J. Photochem. Photobiol., A*, 2023, **440**, 114656.

84 N. Patil, R. Dhake, R. Phalak, U. Fegade, C. Ramalingan, V. Saravanan, Inamuddin and T. Altalhi, A Colorimetric Distinct Color Change Cu(II) 4-{[1-(2,5-dihydroxyphenyl) ethylidene]amino}-1,5-dimethyl-2-phenyl-1,2-dihydro-3H-pyrazol-3-one Chemosensor and its Application as a Paper Test Kit, *J. Fluoresc.*, 2023, **33**, 1089–1099.

85 P. Rasin, S. M. Basheer, J. Haribabu, K. N. Aneesrahman, V. Manakkadan, V. N. Vadakkedathu Palakkeezhillam, N. Bhuvanesh, C. Echeverria, J. F. Santibanez and A. Sreekanth, Host–guest interactions of coumarin-based 1,2-pyrazole using analytical and computational methods: Paper strip-based detection, live cell imaging, logic gates and keypad lock applications, *Heliyon*, 2024, **10**, e24077.

86 X. Li, Z. Meng, S. Gong, Y. Liang, Y. Zhang, Y. Yang, X. Xu, Z. Wang and S. Wang, Development of a novel ratiometric fluorescent probe for real-time monitoring of acidic pH and its applications in food samples and biosystem, *Microchem. J.*, 2024, **204**, 111169.

87 X. Liu, K. Wang, L. Wei, Y. Wang, C. Liu, X. Rong, T. Yan, W. Shu and B. Zhu, A highly sensitive Golgi-targeted fluorescent probe for the simultaneous detection of malondialdehyde and formaldehyde in living systems and foods, *Talanta*, 2024, **278**, 126427.

88 Y. Deng, T. Shen, X. Yu, J. Li, P. Zou, Q. Gong, Y. Zheng, H. Sun, X. Liu and H. Wu, Tetrazine-Isonitrile Bioorthogonal Fluorogenic Reactions Enable Multiplex Labeling and Wash-Free Bioimaging of Live Cells, *Angew. Chem., Int. Ed.*, 2024, **63**, e2023198.

89 C. Krishnamurthy, K. Jathi, K. M. Pallavi and C. Yesudhasan, Hydrazo Pyrazole-Pyridone Fluorescent tag for NLO, Live cell imaging, LFPs visualization, Photophysical probing, and Electrochemical sensor for Dopamine detection, *Luminescence*, 2024, **39**, e4760.